



# CHORUS

This is the accepted manuscript made available via CHORUS. The article has been published as:

## Dynamic instabilities in strongly correlated $VSe_2$ monolayers and bilayers

Marco Esters, Richard G. Hennig, and David C. Johnson

Phys. Rev. B **96**, 235147 — Published 27 December 2017

DOI: [10.1103/PhysRevB.96.235147](https://doi.org/10.1103/PhysRevB.96.235147)

# Dynamic instabilities in strongly correlated VSe<sub>2</sub> monolayers and bilayers

Marco Esters,<sup>1</sup> Richard G. Hennig,<sup>2</sup> and David C. Johnson<sup>1,\*</sup>

<sup>1</sup>*Department of Chemistry, University of Oregon, Eugene, Oregon 97403, USA*

<sup>2</sup>*Department of Materials Science and Engineering,  
University of Florida, Gainesville, Florida 32611, USA*

(Dated: December 6, 2017)

With the emergence of graphene and other two-dimensional (2D) materials, transition metal dichalcogenides have been intensely investigated as potential 2D materials using experimental and theoretical methods. VSe<sub>2</sub> is an especially interesting material since its bulk modification exhibits a charge density wave (CDW), the CDW is retained even for few-layer nanosheets, and monolayers of VSe<sub>2</sub> are predicted to be ferromagnetic. In this work, we show that electron correlation has a profound effect on the magnetic properties and dynamic stability of VSe<sub>2</sub> monolayers and bilayers. Including a Hubbard- $U$  term in the DFT calculations strongly affects the magnetocrystalline anisotropy in the 1T-VSe<sub>2</sub> structure, while leaving the 2H-polytype virtually unchanged. This demonstrates the importance of electronic correlations for the electrical and magnetic properties of 1T-VSe<sub>2</sub>. The Hubbard- $U$  term changes the dynamic stability and the presence of imaginary modes of ferromagnetic 1T-VSe<sub>2</sub> while affecting only the amplitudes in the non-magnetic phase. The Fermi surface of non-magnetic 1T-VSe<sub>2</sub> allows for nesting along the CDW vector, but plays no role in ferromagnetic 1T-VSe<sub>2</sub>. Following the eigenvectors of the soft modes in non-magnetic 1T-VSe<sub>2</sub> monolayers yields a CDW structure with a 4×4 supercell and Peierls-type distortion in the atomic positions and electronic structure. The magnetic order indicates the potential for spin density wave structures.

## I. INTRODUCTION

The discovery of graphene has sparked heightened interest in studying and finding new two-dimensional (2D) materials.<sup>1-3</sup> Apart from graphene, transition metal dichalcogenides (TMDs) have been intensely researched as potential candidates as 2D materials due to their layered structures. TMDs exhibit diverse physical and chemical properties, and reducing dimensionality may yield additional properties due to quantum confinement.<sup>4</sup> Additionally, TMDs are chemically diverse, unlike graphene, which is chemically inert. Thus, while functionalization of graphene leads to the loss of some of its properties, functionalizing TMDs can enhance their properties or create new ones.<sup>5</sup> All these factors make 2D TMDs particularly interesting for applications in electronic and sensing devices, and in catalysis and energy storage. As a result, a large amount of research has been done on 2D TMDs using theoretical and experimental methods such as the transition of MoS<sub>2</sub> from an indirect to a direct semiconductor when reducing the dimensions from bulk and multilayers to a monolayer.<sup>4-16</sup> Magnetic 2D materials are especially interesting due to their potential use in spintronic devices.<sup>17-23</sup> The prediction of magnetic TMD materials has been subject to extensive theoretical investigation, such as the systematic change in magnetic properties through strain,<sup>18,22,24-27</sup> hydrogenation,<sup>27,28</sup> and chemical substitution.<sup>29</sup> Moreover, pristine dichalcogenide monolayers of some first row transition metals (V, Cr, Mn, Fe) are predicted to have magnetic order.<sup>19,20,22,24,26,30-34</sup>

Bulk VSe<sub>2</sub> has been subject to extensive experimental studies due to its ability to intercalate ions<sup>35-39</sup> and its charge density wave (CDW).<sup>40-46</sup> Few-layer VSe<sub>2</sub> nanosheets were successfully synthesized using liquid exfoliation.<sup>47</sup> These nanosheets retain the CDW and the metallic properties of its bulk analog, but their magnetic properties were reported to be different: the sheets are ferromagnetic at room temperature, whereas bulk VSe<sub>2</sub> exhibits temperature independent paramagnetism.<sup>48-50</sup> Isolated monolayers of VSe<sub>2</sub> have not been synthesized yet. However, monolayers of VSe<sub>2</sub> can be found in misfit layer compounds and ferecrystals, where they are sandwiched between monochalcogenides that crystallize in a rock-salt type structure.<sup>51-56</sup> While the existence of CDWs is well documented in ferecrystals and absent in misfit layer compounds, presumably due to structural distortions, the magnetic properties have not been reported for any of these compounds.

In recent years, density functional theory (DFT) calculations were performed on single layer and few layer VSe<sub>2</sub> where the V atoms were coordinated in a distorted octahedral ( $D_{3d}$ , 1T-polytype, Figure 1a) and a trigonal prismatic geometry ( $D_{3h}$ , 2H-polytype, Figure 1b).<sup>24,30,34,57</sup> These calculations predict the ground state of undistorted VSe<sub>2</sub> layers to be the ferromagnetic 2H-polytype with a metal to semimetal/semiconductor transition when going from the bilayer to the monolayer.<sup>30,31,34</sup> The dynamic stability, an important predictor of a charge density wave, was not reported. Strong electron correlation may play an important role in monolayer VSe<sub>2</sub>. Zhuang and Hennig have shown that the strength of electron correlation affects a variety of properties in VS<sub>2</sub>, such as the electronic structure and the stability of the 1T and 2H-polytype.<sup>32</sup> DFT+U calculations by Huang

---

\* davej@uoregon.edu

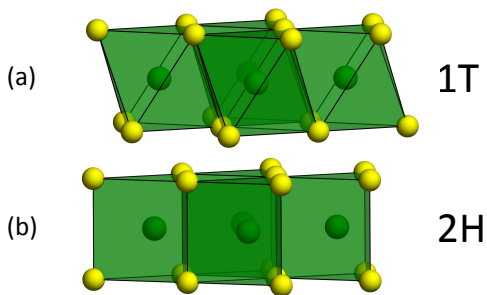


FIG. 1. Structures of monolayer  $VSe_2$  with (a) octahedrally coordinated V as in 1T- $VSe_2$  and (b) trigonally prismatic coordinated V as in the 2H- $VSe_2$  polymorph. Vanadium atoms are shown in light yellow and selenium atoms in dark green.

*et al.* on 2H- $VSe_2$  monolayers have shown that electron correlation in 2H- $VSe_2$  greatly influences the electronic structure.<sup>57</sup>

This work presents DFT calculations to explore correlation effects in monolayer and bilayer  $VSe_2$ . It will be shown that electron correlation has profound effects on the magnetic properties, electronic structure, and dynamic stability of the 1T-polytype. First, the van der Waals functionals and the Hubbard- $U$  parameter will be benchmarked against the in-plane lattice parameter in ferecrystals. These parameters will be used to determine the magnetic ground state(s) of  $VSe_2$  monolayers and bilayers, and to examine the effect of the Hubbard parameter on the electronic structure. At last, we will show that  $VSe_2$  is not dynamically stable and predict a CDW structure with a Peierls-like distortion and a ferromagnetic ground state.

## II. COMPUTATIONAL METHODS

All DFT calculations were performed using the Vienna ab initio simulation package (VASP).<sup>58-60</sup> The interactions between the ionic core and the valence electrons were described using the projector-augmented wave (PAW) method using a cutoff energy of 500 eV.<sup>61,62</sup> The  $3p^63d^4s^1$  and the  $4s^24p^4$  states were used as valence electrons for V and Se, respectively. For the exchange-correlation functional, we compare results for the local-density approximation (LDA)<sup>63</sup>, the Perdew-Burke-Ernzerhof (PBE)<sup>64</sup> generalized-gradient approximation (GGA), and the Heyd-Scuseria-Ernzerhof (HSE06) hybrid method with the standard exact-exchange mixing parameter of  $\alpha = 0.25$ .<sup>65</sup> For the Hubbard- $U$  term, Dudarev's approach was used to treat localized  $d$ -orbitals in V, using the effective  $U$  parameter,  $U_{\text{eff}} = U - J$ , with  $U$  and  $J$  being the on-site Coulomb and exchange parameters, respectively.<sup>66</sup> Since the interactions between individual  $VSe_2$  layers is of van der Waals type, dispersion corrections were included for the GGA functionals using the method of Tkatchenko and Scheffler

(TS), Grimme's DFT-D2 method, and Dion's method in the vdW-DF corrected optPBE, optB86b and optB88 functionals.<sup>67-74</sup> Brillouin zone integration was carried out using a  $\Gamma$ -centered k-point grid with a high k-point density of approximately 60 k-points per  $\text{\AA}^{-1}$ .<sup>75</sup> Atomic positions and lattice parameters were fully optimized until the forces were smaller than 0.01 eV/ $\text{\AA}$  and the stresses smaller than 0.05 GPa. A vacuum of 30  $\text{\AA}$  was included for the monolayer and bilayer calculations to minimize interactions between periodic images. For total energy calculations, self-consistency was achieved with an energy convergence of  $10^{-6}$  eV. The magnetic anisotropies were obtained by including spin-orbit interactions in a non-selfconsistent calculation using charge and spin densities from calculations without spin-orbit interactions. Since magnetic anisotropies can be in the sub-meV regime, an energy convergence of  $10^{-8}$  eV was used for these calculations. Band structures were visualized and  $VSe_2$  slabs were generated using the open source PYTHON packages PYMATGEN in conjunction with MPINTERFACES.<sup>76,77</sup> Spin densities were visualized with the program VESTA.<sup>78</sup> Fermi surfaces were calculated using the Wannier interpolation as implemented in the WANNIER90 code and visualized using XCRYSDEN.<sup>79,80</sup>

## III. RESULTS AND DISCUSSION

### A. Stability of undistorted $VSe_2$ layers with different coordination geometries

Figure 2a shows the differences in formation energy,  $\Delta E$ , between  $VSe_2$  monolayers in the octahedral (1T) and trigonal prismatic (2H) structure as a function of the Hubbard- $U$ .  $\Delta E$  depends strongly on the exchange correlation functional,  $U_{\text{eff}}$ , and the van der Waals functional, similar to the findings for  $VS_2$ .<sup>32</sup> For all functionals,  $\Delta E$  exhibits a maximum value at intermediate values of  $U_{\text{eff}}$ . For the GGA functional, PBE and the van der Waals corrected GGA functionals vdW-optPBE, vdW-optB88, vdW-optB86b, TS-GGA, and GGA-D2, the maximum occurs at a lower  $U_{\text{eff}}$  of 0.5 to 1.0 eV compared to a  $U_{\text{eff}}$  of 2.5 eV for the LDA functional. This is similar to the behavior and values observed for  $VS_2$ .<sup>32</sup> For most functionals, the maximum value for  $\Delta E$  agrees well with the value for HSE06 of 41 meV per formula unit (f.u.), except for the DFT-D2 and the Tkatchenko-Scheffler van der Waals functionals. For the GGA+ $U$  methods, the 2H-structure is stable for  $U_{\text{eff}}$  below about 2 eV. For the LDA+ $U$  method, 1T is stable for  $U_{\text{eff}}$  below 0.5 eV and above 3.5 eV. These trends are similar for the bilayer and the bulk (see Figures S2 and S3 in the Supplemental Material<sup>81</sup>). Isaacs and Marianetti attributed these changes in energy for  $VS_2$  to an increased filling and ordering of the V  $d$ -orbitals in 1T- $VS_2$ , and we observe the same trends in the density matrix elements for  $VSe_2$ .<sup>82</sup>

The magnetization  $m$  of the 1T monolayer as a func-

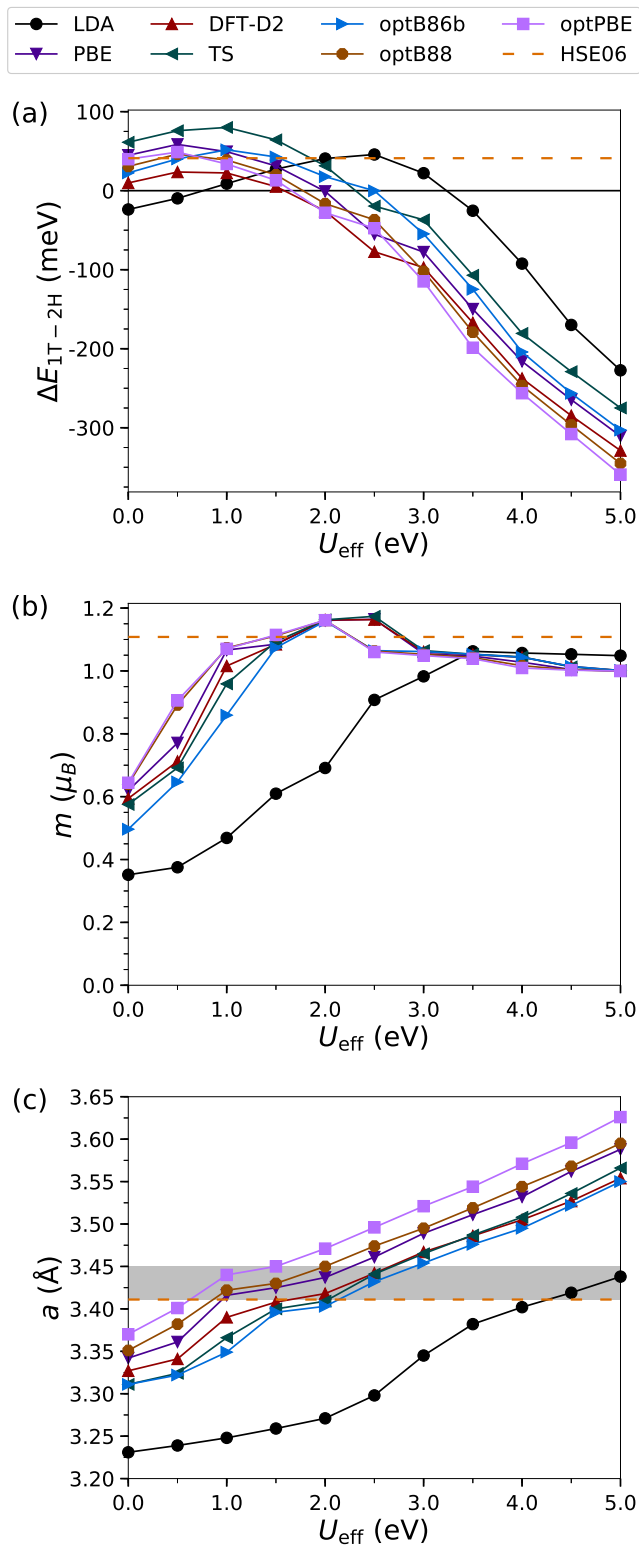


FIG. 2. (a) Energy difference  $\Delta E$  between 1T and 2H-VSe<sub>2</sub> monolayers as a function of  $U_{\text{eff}}$ , exchange-correlation and van der Waals functional. Positive  $\Delta E$  indicates that 2H is more stable. (b) Magnetization  $m$  of monolayer 1T-VSe<sub>2</sub> as a function of  $U_{\text{eff}}$ , exchange-correlation and van der Waals functional. (c) In-plane lattice parameters  $a$  of monolayer 1T-VSe<sub>2</sub>. The gray shades represent the range of experimental values found for ferrocystals.

TABLE I. Lattice parameters of the relaxed bulk structure of 1T-VSe<sub>2</sub> with  $U_{\text{eff}} = 1.0$  eV using standard PBE, vdW-DF-optPBE, and vdW-DF-optB88 functionals.

	Experiment <sup>48-50</sup>	PBE	optPBE	optB88
$a$ (Å)	3.35	3.42	3.46	3.44
$c$ (Å)	6.10	6.84	6.30	6.13
$c/a$	1.82	2.00	1.82	1.78

tion of  $U_{\text{eff}}$  is pictured in Figure 2b. The magnetization of the 1T-polytype is very sensitive to  $U_{\text{eff}}$ , and for low  $U_{\text{eff}}$ , also to the choice of van der Waals correction. Using LDA, the magnetization gradually increases until it plateaus at  $1.05 \mu_B$  at  $U_{\text{eff}} = 3.5$  eV. For PBE, the magnetization reaches a maximum of  $1.15 \mu_B$  at  $U_{\text{eff}} = 2.5$  eV and then decreases to unity. While LDA+U shows lower magnetization compared to the HSE06 functional, the magnetization of the GGA+U calculations coincide with HSE06 at  $U_{\text{eff}} = 1.5$  eV, regardless of the van der Waals functional. PBE without dispersion correction, and the optPBE and optB88 functionals already coincide with HSE06 at  $U_{\text{eff}} = 1.0$  eV. For 2H (Figure S1c), the magnetization is at unity using HSE06 and PBE, regardless of  $U_{\text{eff}}$  and van der Waals functional, whereas LDA reaches the same value at  $U_{\text{eff}} = 1.5$  eV.

Since isolated monolayers of VSe<sub>2</sub> have not been synthesized yet, finding a good benchmark to decide on an exchange-correlation functional and a value for  $U_{\text{eff}}$  is challenging. However, ferrocystals contain monolayers of transition metal dichalcogenides and can be used as an approximation. The compounds [(MSe)<sub>1+ $\delta$ ] <sub>$m$</sub> [VSe<sub>2</sub>]<sub>1</sub> (M = Pb, Sn) have a relatively constant  $a$ -axis lattice parameter of  $a = 3.42$  Å, regardless of  $m$ , the thickness of the MSe layer.<sup>52-56,83</sup> The in-plane lattice parameter  $a$  of the isolated VSe<sub>2</sub> monolayers calculated with different functionals are shown in Figure 2c. For all functionals, the  $a$ -axis lattice parameter increases with increasing  $U_{\text{eff}}$ . As the figure shows, adding a Hubbard- $U$  is necessary to reach the experimental in-plane lattice parameter. LDA agrees with experiments only at  $U_{\text{eff}} = 4.5$  eV. optB86b, DFT-D2, and the Tkatchenko-Scheffler functionals need a moderately high  $U_{\text{eff}}$  of 2.5 eV whereas PBE, optPBE and optB88 only need 1 eV to agree with the experimental lattice parameters. HSE06 underestimates the  $a$ -axis lattice parameters only slightly. It is clear to see that any functional can reproduce these lattice parameters with a high enough value of  $U_{\text{eff}}$ .</sub>

For monolayers, one would expect van-der-Waals forces to be negligible, and the results should coincide well with the PBE functional without dispersion corrections, which is only true for optPBE and optB88. Since optPBE showed much more stable convergence behavior and also gave a more accurate  $c/a$  ratio for the bulk (see Table I), we decided that optPBE with  $U_{\text{eff}} = 1.0$  eV is the most suitable functional. We cross-checked select results with calculations using the optB86b functional and

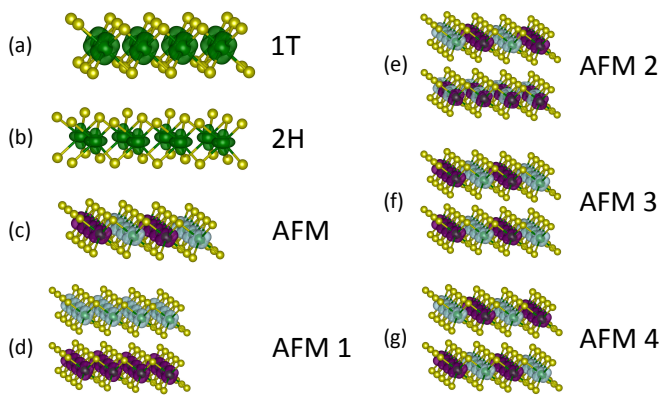


FIG. 3. Spin densities for  $VSe_2$  layers. (a) 1T- $VSe_2$  monolayer with ferromagnetic (FM) spin structure. (b) 2H- $VSe_2$  monolayer with FM spin structure. (c) 1T- $VSe_2$  monolayer with antiferromagnetic (AFM) spin orientation. (d – g) 1T- $VSe_2$  bilayer with AFM ordering (AFM 1 – AFM 4). For 2H- $VSe_2$ , AFM 3 and AFM 4 are identical. For AFM structures, light red and dark blue spin densities denote opposite spin orientations. The isosurface values are set to  $0.01 e/a_0^3$  where  $a_0$  is the Bohr radius.

$U_{\text{eff}} = 2.5$  eV, which also reproduces the experimental in-plane geometry well. The strong dependence of the lattice geometry, magnetic properties, and relative phase stability on  $U_{\text{eff}}$  and the van der Waals functional may indicate that more advanced methods such as dynamic mean field theory may be necessary to completely describe  $VSe_2$ .

It is important to note that PBE predicts bulk 1T- $VSe_2$  to be ferromagnetic even though it exhibits temperature-independent paramagnetism in experiments, and should thus converge to a non-magnetic state. Using mean field theory, we estimated the Curie temperature of the bulk structure to be approximately 39 K and 17 K without a Hubbard- $U$  and with  $U_{\text{eff}} = 1.0$  eV, respectively, which is significantly below the charge density transition temperature of 100 – 110 K (see Table S1 and the corresponding text in the Supplemental Information).<sup>40–46</sup> A ferromagnetic ground state is thus not inconsistent with experimental evidence since undistorted 1T- $VSe_2$  is not stable in the temperature regime in which it would be ferromagnetic.

### B. Magnetic structure of 1T- $VSe_2$ and 2H- $VSe_2$

There are various configurations of magnetic order possible for the single and bilayer 1T and 2H-polytypes of  $VSe_2$ . Figure 3 shows the spin densities for the ferromagnetic (FM) and different antiferromagnetic (AFM) configurations of  $VSe_2$  monolayers and bilayers. For the single layer polytypes, the striped AFM order in Figure 3c is considered. Four different AFM configurations are considered for the bilayer polytypes and illustrated in Figure 3d – g for the bilayer 1T-structure. They include

configurations of parallel spins in each layer in Figure 3d, striped configurations where the stripes are oriented perpendicular in Figure 3e, oriented parallel in a staggered pattern in Figure 3f, and in an eclipsing pattern in Figure 3g. Equivalent patterns are considered for the bilayer 2H-structure. Due to the different stacking in the 2H-polytype, the AFM 3 and AFM 4 configurations are identical in 2H- $VSe_2$  bilayers.

Table II shows the energies of the various possible types of magnetic order in the single and bilayer 1T and 2H-polytypes ( $U_{\text{eff}} = 1.0$  eV). Overall, the magnetic configurations are strongly favored, indicating the tendency of  $VSe_2$  layers to exhibit some form of magnetic order. Similar to the results of Wasey *et al.* using PBE-D2 without a Hubbard- $U$ ,<sup>31</sup> monolayer  $VSe_2$  is ferromagnetic for both polytypes. As illustrated in Figure 3, the spin densities around the V atom show  $a_{1g}$  symmetry for the 1T-polytype and  $a'_1$  symmetry for the 2H-polytype (the  $d_{z^2}$  orbital). For bilayers, the energy of the anti-ferromagnetic order with ferromagnetic intra-layer (AFM 1) coupling is nearly identical to the ferromagnetic order whereas the structures with anti-ferromagnetic intra-layer coupling (AFM 2 – AFM 4) have substantially higher energies. This suggests that there is a strong intra-layer exchange coupling and virtually no inter-layer exchange coupling. The magnetic order of  $VSe_2$  multilayers could thus be ferromagnetic or antiferromagnetic, or could show various disordered spin structures along the  $c$ -axis with ferromagnetic  $VSe_2$  sheets. The AFM energies for 1T- $VSe_2$  are substantially lower than for 2H- $VSe_2$ , suggesting much weaker intra-layer exchange coupling in the 1T-structure.

### C. Effect of the electron correlation strength on the electronic structure of $VSe_2$ layers

Introducing the Hubbard- $U$  parameter has profound effects on the structure of 1T- $VSe_2$  whereas the 2H-polytype remains virtually unaffected. Table III shows the structural and magnetic parameters of the relaxed monolayers and bilayers in their ground states. For 2H- $VSe_2$ , the lattice parameters increase only slightly by 0.1 Å when  $U_{\text{eff}}$  is increased to 1.0 eV and there is no change in lattice parameters when going from the monolayer to the bilayer. The distance between the Se and V planes also remain unchanged, and the magnetization is approximately unity regardless of Hubbard parameter, number of layers and magnetic structure. For V and Se, the magnitude of the magnetization increases only slightly as well. For 1T- $VSe_2$ , increasing  $U_{\text{eff}}$  to 1.0 eV leads to a “flattening” of the monolayer by increasing the in-plane lattice parameter and decreasing the distance between the Se and V planes. For the bilayer, the same trend can be seen, but there is also a small increase in the distance between  $VSe_2$  layers.

The in-plane lattice parameters are in good agreement with the experimental values for ferecrystals, and are

TABLE II. Energy differences  $\Delta E_{\text{mag}}$  in meV per formula unit with reference to the ferromagnetic order for the non-magnetic (NM) and anti-ferromagnetic (AFM) configurations using  $U_{\text{eff}} = 1.0$  eV. For the bilayer, four and three different anti-ferromagnetic cells can be created for the 1T and 2H-polytype, respectively.

Polytype	Monolayer		Bilayer				
	NM	AFM	NM	AFM 1	AFM 2	AFM 3	AFM 4
1T	97	25	94	2	25	24	25
2H	157	106	148	-1	102	102	—

TABLE III. Comparison of the structural parameters, and magnetic moments for isolated VSe<sub>2</sub> monolayers and bilayers with and without the Hubbard parameter  $U_{\text{eff}} = 1.0$  eV. The structural parameters include the in-plane lattice parameter  $a$ , the distance between the V and Se planes  $d(\text{V-Se})$ , and the distance between the two VSe<sub>2</sub> layers in the bilayer  $d(\text{VSe}_2\text{-VSe}_2)$ . The magnetic moments  $m$  are given for the unit cell ( $m_{\text{cell}}$ ), and for the contributions from the V and Se atoms  $m(\text{V})$  and  $m(\text{Se})$ , respectively.  $\Delta E$  denotes the energy difference between the 1T and 2H polytype (positive when 2H is more stable).

Monolayer										
Polytype	$U_{\text{eff}} = 0$ eV				$U_{\text{eff}} = 1.0$ eV					
	1T	2H	1T	2H	1T	2H	1T	2H		
$a$ (Å)	3.370	3.363	3.441	3.375						
$d(\text{V-Se})$ (Å)	1.581	1.606	1.559	1.608						
$m_{\text{cell}}$ ( $\mu_{\text{B}}$ )	0.64	1.00	1.07	1.00						
$m(\text{V})$ ( $\mu_{\text{B}}$ )	0.69	1.00	1.27	1.10						
$m(\text{Se})$ ( $\mu_{\text{B}}$ )	-0.05	-0.07	-0.13	-0.10						
$\Delta E_{1\text{T}-2\text{H}}$ (meV)	39				33					

Bilayer										
Magnetic order	$U_{\text{eff}} = 0$ eV				$U_{\text{eff}} = 1.0$ eV					
	FM	AFM 1	FM	AFM 1	FM	AFM 1	FM	AFM 1		
Polytype	1T	2H	1T	2H	1T	2H	1T	2H	1T	2H
$a$ (Å)	3.379	3.367	3.376	3.367	3.447	3.378	3.446	3.379		
$d(\text{V-Se})$ (Å)	1.582	1.608	1.584	1.609	1.559	1.611	1.560	1.610		
$d(\text{VSe}_2\text{-VSe}_2)$ (Å)	1.574	1.601	1.574	1.601	1.553	1.607	1.554	1.605		
$d(\text{VSe}_2\text{-VSe}_2)$ (Å)	3.252	3.337	3.245	3.307	3.230	3.393	3.261	3.334		
$m/\text{f.u.}$ ( $\mu_{\text{B}}$ )	0.66	0.98	0.00	0.00	1.07	1.00	0.00	0.00		
$m(\text{V})$ ( $\mu_{\text{B}}$ )	0.71	0.99	$\pm 0.68$	$\pm 1.01$	1.27	1.10	$\pm 1.27$	$\pm 1.01$		
$m(\text{Se})$ ( $\mu_{\text{B}}$ )	-0.05	-0.07	$\pm 0.05$	$\pm 0.07$	-0.13	-0.10	$\pm 0.13$	$\pm 0.10$		
$\Delta E_{1\text{T}-2\text{H}}/\text{f.u.}$ (meV)	32		32		22		25			

larger than in the bulk.<sup>48–56,83</sup> The magnetization increases significantly from  $0.6 - 0.7 \mu_{\text{B}}$  to slightly above unity. This is mostly due to the strong increase of the magnetic moment of the V atom, which almost doubles. Although the magnetic moments of the Se atoms, which are oriented antiparallel to the moments the V atoms, increase as well, they are much smaller in magnitude. The energy of the 1T-polytype decreases with respect to the 2H-polytype, but 2H is still the ground state.

The band structures with  $U_{\text{eff}} = 1.0$  eV of the ferromagnetic monolayers and bilayers and the AFM 1 bilayer structures are shown in Figure 4. Ferromagnetic 1T-VSe<sub>2</sub> is a metal where the Fermi level consists of a minority-spin hole-like part centered around the  $\Gamma$  point and a majority-spin electron-like part centered around

the M point. Going from the monolayer to the bilayer doubles the number of bands, and the additional bands are degenerate with the bands of the monolayer, except for the highest occupied band near the  $\Gamma$  point where splitting can be observed. This splitting brings the highest occupied band near the  $\Gamma$  point closer to the Fermi level compared to the monolayer, almost to the same energy as the bands at the K point. This has been observed in other TMDs when transitioning from monolayers to bilayers and is due to the introduction of anti-bonding intra-layer interactions.<sup>4,8,31,84–86</sup> Whereas for example in MoS<sub>2</sub>, this phenomenon leads to a transition from a direct to an indirect semiconductor, the increase in energy is not sufficient to change the electrical properties in 1T-VSe<sub>2</sub>. The band structure of the antiferromag-

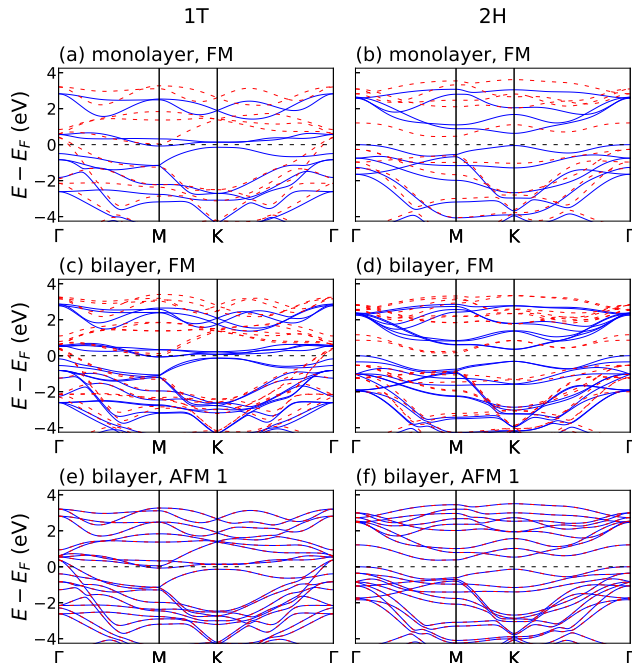


FIG. 4. Spin-polarized band structures for 1T-VSe<sub>2</sub> (left) and 2H-VSe<sub>2</sub> (right) layers with  $U_{\text{eff}} = 1.0$  eV. (a, b) Ferromagnetic monolayer; (c, d) ferromagnetic bilayer; (e, f) bilayer with AFM 1 structure. Solid blue lines correspond to majority and red dashed lines to minority spin bands.

netic 1T-VSe<sub>2</sub> bilayer is essentially identical to the sum of two ferromagnetic band structures with opposite spins, providing further evidence that the electronic coupling between individual VSe<sub>2</sub> layers is very small. Similar behavior is observed for the band structures of the 2H-VSe<sub>2</sub> monolayers and bilayers. The FM 2H-VSe<sub>2</sub> monolayer is a semiconductor with an indirect gap between  $\Gamma$  and M and a slightly larger direct band gap at the K point. 2H-VSe<sub>2</sub> remains an indirect semiconductor in the FM bilayer. The transition from semiconductor to metal reported in the literature<sup>31</sup> does not occur when the Hubbard- $U$  is included in the description. Similar to bilayer 1T-VSe<sub>2</sub>, the electronic coupling between the layers in 2H-VSe<sub>2</sub> layers is very small.

Crystal field theory predicts that the  $d$ -orbitals in the 2H-polytype with  $D_{3h}$  symmetry around the V atom split into  $e'$  and  $e''$  orbitals, each doubly degenerate, and one  $a'_1$  orbital. For the 1T-polytype, the V atom is coordinated in a  $D_{3d}$  symmetry and should split into two sets of doubly degenerate  $e_g$  orbitals, and one  $a_{1g}$  orbital. The orbital-projected band structures of the monolayers in Figure 5 show this splitting at the  $\Gamma$  point for both polytypes with the energies increasing from  $e'$  ( $d_{xy} + d_{x^2-y^2}$ ) to  $e''$  ( $d_{xz} + d_{yz}$ ) and  $a'_1$  ( $d_{z^2}$ ), and from both  $e_g$  orbitals ( $d_{xy} + d_{x^2-y^2}$ ) and ( $d_{xz} + d_{yz}$ ) to  $a_{1g}$  ( $d_{z^2}$ ) for 2H-VSe<sub>2</sub> and 1T-VSe<sub>2</sub>, respectively. Just as in VS<sub>2</sub>,<sup>32</sup> the  $e'$  and  $e''$  orbitals strongly hybridize with the Se orbitals

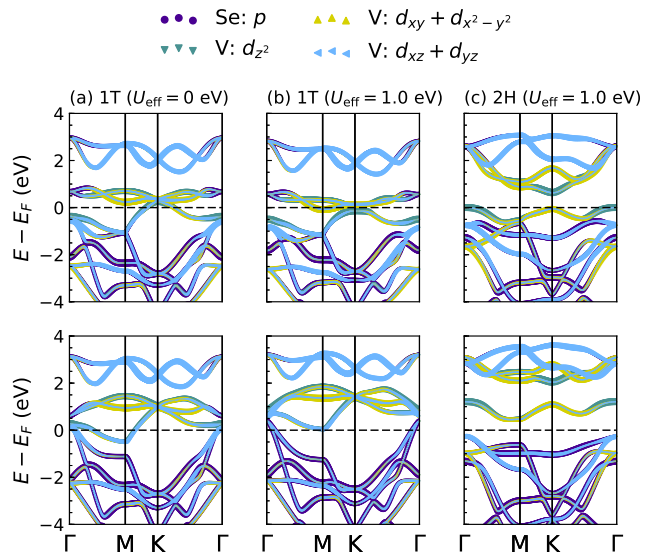


FIG. 5. Orbital resolved majority spin (top) and minority spin (bottom) band structures of monolayer VSe<sub>2</sub>. (a) 2H-VSe<sub>2</sub> with  $U_{\text{eff}} = 1.0$  eV; (b) 1T-VSe<sub>2</sub> with  $U_{\text{eff}} = 0$  eV; (c) 1T-VSe<sub>2</sub> with  $U_{\text{eff}} = 1.0$  eV.

whereas the  $a'_1$  orbital only hybridizes to a small degree. At the Fermi level, the bands are predominantly of  $a'_1$  ( $\Gamma$  point) and  $e'$  (K point) character, which is consistent with the shape of the spin density shown in Figure 3b (the  $e'$  orbitals are masked by the “ring” of the  $d_{z^2}$  orbital). While changes in  $U_{\text{eff}}$  have only negligible effects on the band structure on the 2H polytype, they have strong effects on the band structure of 1T-VSe<sub>2</sub>. Figures 5a and b show that these effects are mostly found at the M and the K point for the majority spin bands, and at the M point for the minority spin bands. At the M point, the majority spin  $e_g$  band that consists of the  $d_{xy}$  and  $d_{x^2-y^2}$  orbitals is lowered in energy and crosses the Fermi level. Near the K point, a majority spin band with  $d_{z^2}$  and partial  $e_g$  character crosses the Fermi level for  $U_{\text{eff}} = 0$  eV, whereas for  $U_{\text{eff}} = 1.0$  eV, the band maximum is shifted below the Fermi level at the K point. This changes the character of the Fermi surface from hole-like at K for  $U_{\text{eff}} = 0$  eV to electron-like at M for  $U_{\text{eff}} = 1.0$  eV. The minority spin band structures show that at the M point, the  $e_g$  band, which is comprised of the V  $d_{xz}$  and  $d_{yz}$  orbitals, is raised above the Fermi energy. The same band is also raised in energy at the  $\Gamma$  point. Another consequence is that the minority spin bands that cross the Fermi level near the  $\Gamma$  point are of significantly less  $e_g$  character, and remain predominantly of Se  $p$  character. At the  $\Gamma$  point, the Se  $p$  orbital is also lowered in energy with respect to the  $e_g$  and  $a_{1g}$  orbitals. This explains the increased magnetization of 1T-VSe<sub>2</sub> with increased  $U_{\text{eff}}$ .

These changes can also be observed at the Fermi surfaces (Figure 6). Without a Hubbard- $U$ , there are Fermi surface pockets around all high symmetry points. The majority spin bands form almost triangular shaped hole

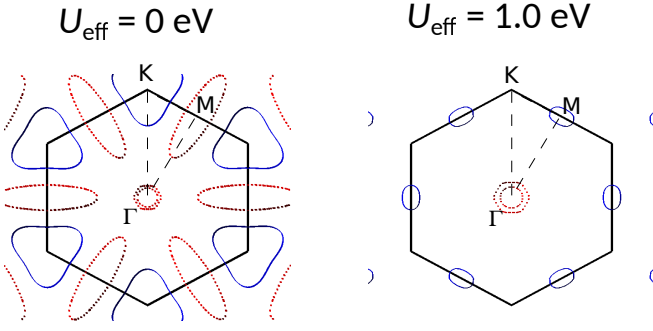


FIG. 6. Fermi surfaces of ferromagnetic 1T-VSe<sub>2</sub> monolayers for  $U_{\text{eff}} = 0$  eV and  $U_{\text{eff}} = 1.0$  eV. Solid blue surfaces are from the majority spin bands and red dashed surfaces are from the minority spin bands. The edges of the Brillouin zone are shown in black solid lines, and the edges of the irreducible Brillouin zone are shown in black dashed lines.

pockets around the K point. The surfaces at neighboring K points are almost parallel to each other, which may result in Fermi surface nesting. Fermi surface nesting is often cited as a cause for charge density waves, but this may not necessarily be the case, as we will discuss in Section III D.<sup>87,88</sup> The minority spin bands form cigar shaped electron pockets around the M point that point towards the Brillouin zone center where two circular hole pockets of the minority spin bands can be found. Increasing  $U_{\text{eff}}$  to 1.0 eV changes the Fermi surface dramatically. The hole pockets at the K point completely disappear, and the cigar shaped minority spin electron pockets get replaced by small oval majority spin electron pockets that point towards the K points. The hole pockets at the  $\Gamma$  point increase in size, but overall, the size of the Fermi surface pockets decreases, reducing the intrinsic carrier concentration of the monolayer. Fermi surface nesting is not possible anymore for  $U_{\text{eff}} = 1.0$  eV.

For optB86b and  $U_{\text{eff}} = 2.5$  eV (see Figure S4 in the Supplemental Material), the energy of the highest occupied majority spin band decreases further in energy at the K point due to an increased population of the  $d_{z^2}$  orbital. In turn, the minority spin band that is just below the Fermi level at the M point for  $U_{\text{eff}} = 0$  eV is now completely above the Fermi energy. This decreases the size of the Fermi surface pockets, showing that the electrical and magnetic properties are sensitive to the value of the Hubbard- $U$  and not just to the structure. The sensitivity of the carrier type and carrier concentration of the different spin channels suggest that not only strain engineering, but also charge screening can be used to tune the electrical and magnetic properties of VSe<sub>2</sub> layers. The latter could be achieved by using a suitable substrate or by incorporating VSe<sub>2</sub> into heterostructures. For example, in the ferecrystalline alloy [(Sn<sub>1-x</sub>Bi<sub>x</sub>Se)<sub>1+ $\delta$</sub> ][VSe<sub>2</sub>], the  $a$ -axis lattice parameter of the VSe<sub>2</sub> monolayer increases systematically with increasing  $x$ , analogous to the trend observed in Figure 2c for increasing  $U_{\text{eff}}$ .<sup>89</sup>

Spin-orbit coupling (SOC) was introduced to deter-

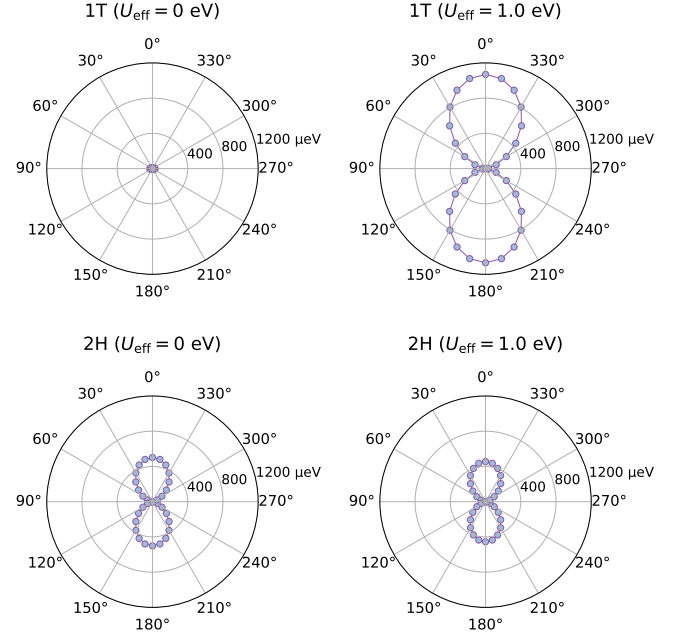


FIG. 7. Angular dependence of the magnetocrystalline anisotropy energy (MAE) with polar angle for monolayer VSe<sub>2</sub>. 0° points along the positive  $z$  axis.

mine the magnetocrystalline anisotropy energy (MAE) of the VSe<sub>2</sub> monolayers. The out-of-plane MAE is shown in Figure 7. Here again, correlation has a strong effect on the 1T-polytype whereas the 2H-polytype is virtually unchanged. Without introducing the Hubbard parameter, 1T-VSe<sub>2</sub> is nearly isotropic. For  $U_{\text{eff}} = 1.0$  eV, however, 1T-VSe<sub>2</sub> monolayers show a large MAE of about 1.1 meV. This is consistent with the MAE obtained with the optB86b functional and  $U_{\text{eff}} = 2.5$  eV where the MAE was 1.2 meV. For 2H-VSe<sub>2</sub>, the MAE only weakly depends on  $U_{\text{eff}}$ . It is much smaller than the MAE of 1T-VSe<sub>2</sub> with 0.46 meV. The 1T and 2H structure both exhibit an easy magnetization plane and belong to the family of  $XY$  magnets. This means that a Berezinsky-Kosterlitz-Thouless transition could be observed at a critical temperature that can be estimated from a classical  $XY$  model as  $T_c = 0.89 J k_B^{-1}$ , where  $J$  is the exchange integral and  $k_B$  the Boltzmann constant. The exchange integral  $J$  can be estimated from the energy difference of the FM and AFM configuration,  $\Delta E_{\text{mag}} = 8J$ .<sup>90</sup>  $T_c$  computes to 137 K for the 2H-polytype. For the 1T-polytype,  $T_c$  is predicted to be 35 K for optPBE and  $U_{\text{eff}} = 1.0$  eV, and 14 K for optB86b and  $U_{\text{eff}} = 2.5$  eV ( $\Delta E_{\text{mag}} = 11$  meV), which is below the experimentally observed charge density wave (CDW) transition temperature of 100 – 110 K (onset).<sup>40–46,52–56</sup> This means that the magnetic transformation in the 1T-structure is unlikely to be observable as the 1T-polytype is unstable at such low temperatures.

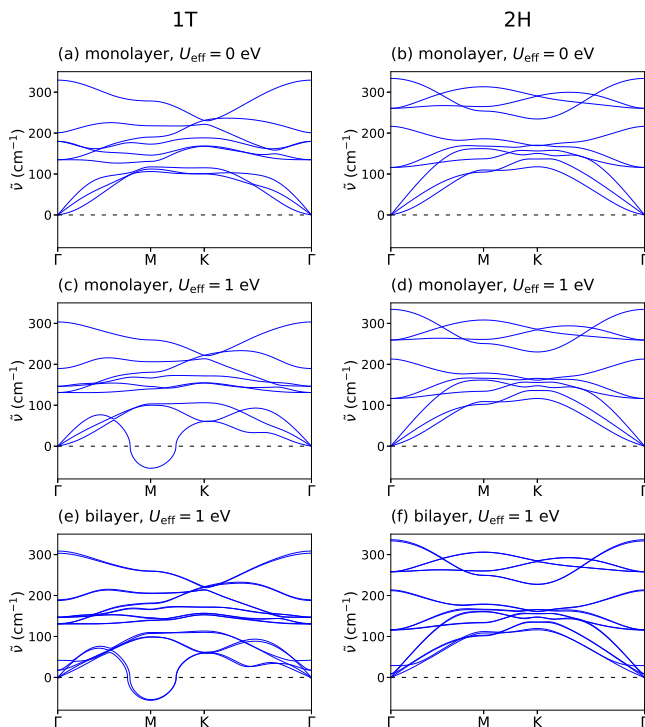


FIG. 8. Phonon dispersion curves for spin-polarized 1T-VSe<sub>2</sub> (left) and 2H-VSe<sub>2</sub> (right) layers. (a,b) Monolayer with  $U_{\text{eff}} = 0$  eV; (c,d) monolayer with  $U_{\text{eff}} = 1.0$  eV; (e,f) bilayer with  $U_{\text{eff}} = 1.0$  eV.

#### D. Dynamic stability of VSe<sub>2</sub> layers

VSe<sub>2</sub> exhibits a charge density wave in bulk, nanosheets and ferecrystals. Density functional perturbation theory (DFPT) as implemented in VASP and the analysis program PHONOPY<sup>91</sup> was used to calculate phonon dispersion relations for the monolayer and bilayer structures. For these calculations, the structures were relaxed until forces on the ions were below 0.001 Å/s. Phonon dispersion curves were also calculated for the bulk 1T-polytype (Figure S5 in the Supplemental Material). The soft modes for the bulk agree with the charge density wave supercell found in experiments, confirming that our functional choice was reasonable.<sup>46,92–95</sup>

The phonon dispersion curves of the ferromagnetic ground states were calculated using a  $4 \times 4$  supercell and are displayed in Figure 8. For  $U_{\text{eff}} = 0$  eV, the monolayers of VSe<sub>2</sub> are dynamically stable for both polytypes even though the Fermi surface (Figure 6) allows for nesting, showing that Fermi surface nesting does not necessarily lead to dynamic instabilities. Increasing  $U_{\text{eff}}$  to 1.0 eV causes imaginary frequencies to appear at the M point for the monolayer of 1T-VSe<sub>2</sub> whereas the monolayer of 2H-VSe<sub>2</sub> remains dynamically stable. The dispersion curves for the bilayer are similar to curves for the monolayer, suggesting that the dynamic instabilities in the bilayer have the same origin as in the monolayer.

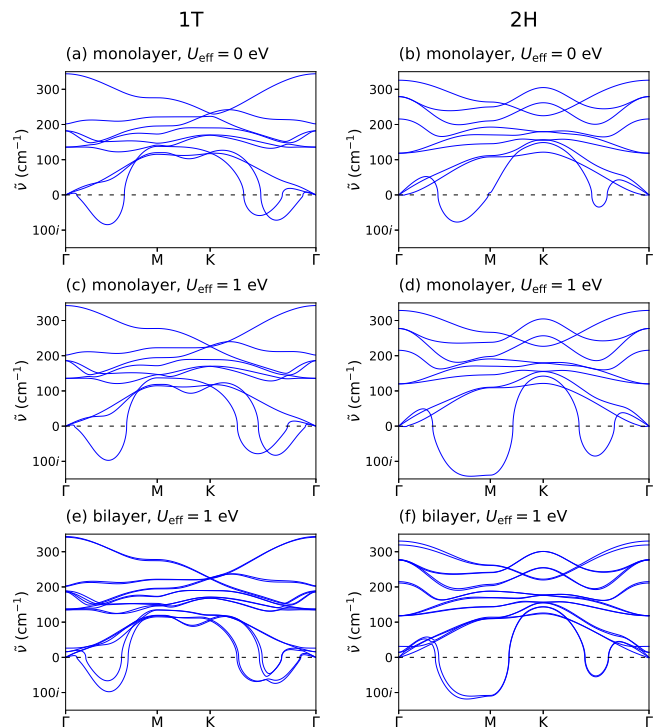


FIG. 9. Phonon dispersion curves for non-magnetic 1T-VSe<sub>2</sub> (left) and 2H-VSe<sub>2</sub> (right) layers. (a,b) Monolayer with  $U_{\text{eff}} = 0$  eV; (c,d) monolayer with  $U_{\text{eff}} = 1.0$  eV; (e,f) bilayer with  $U_{\text{eff}} = 1.0$  eV.

The soft node is at the  $\mathbf{q}$ -point  $(\frac{1}{2}, 0)$  and its symmetry equivalent points. The Fermi surface for  $U_{\text{eff}} = 1.0$  eV shows no parallel surfaces along a vector that corresponds to these points, so Fermi surface nesting cannot be the cause for these imaginary phonon nodes. The soft mode corresponds to either a  $2 \times 1$  or  $2 \times 2$  supercell, which is only half of what was found experimentally for bulk 1T-VSe<sub>2</sub>.<sup>46,92–95</sup> Using optB86b and  $U_{\text{eff}} = 2.5$  eV (Figure S6a in the Supplemental Material) yields no imaginary phonon modes, which shows that the dynamic stability of spin-polarized 1T-VSe<sub>2</sub> is sensitive to the value of  $U_{\text{eff}}$ .

As elaborated in the previous section, the CDW transition temperature for 1T-VSe<sub>2</sub> is above the predicted magnetic transition temperature, so the structural instabilities may be better described using the non-magnetic structure. The phonon dispersion curves of non-spin-polarized VSe<sub>2</sub> layers are shown in Figure 9. The 1T polytype has a soft mode at  $(\frac{1}{4}, 0)$  (or  $\frac{1}{2}M$ ), which is consistent with a  $4 \times 4$  supercell as observed for bulk 1T-VSe<sub>2</sub>. Additional phonon modes with lower imaginary frequency appear at  $(\frac{1}{6}, \frac{1}{6})$  (or  $\frac{1}{2}K$ ), and  $(\frac{1}{8}, \frac{1}{8})$  (or  $\frac{3}{8}K$ ). The frequencies increase with increasing  $U_{\text{eff}}$ , indicating that stronger electron localization destabilizes the lattice more. Comparison with optB86b at  $U_{\text{eff}} = 2.5$  eV confirms this trend (Figure S6b). The node at  $\frac{1}{2}K$  increases stronger in frequency with  $U$  than then node at  $\frac{3}{8}K$ , but

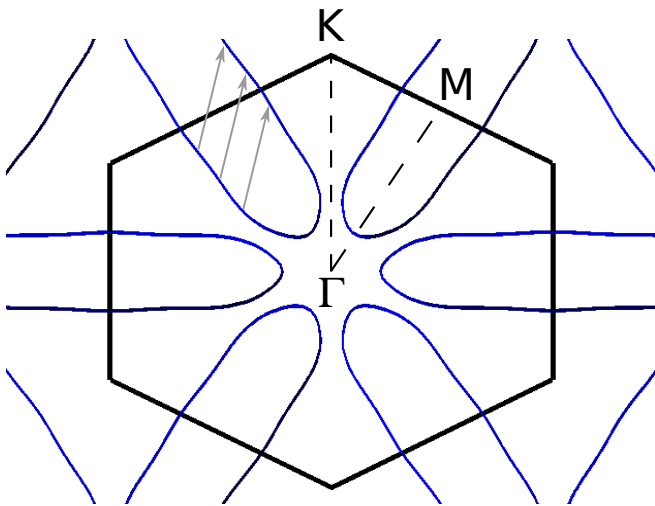


FIG. 10. Fermi surface of a non-spin-polarized 1T-VSe<sub>2</sub> monolayer. The edges of the Brillouin zone are shown in black solid lines, and the edges of the irreducible Brillouin zone are shown in black dashed lines. Nesting vectors are shown in gray.

the node at  $\frac{1}{2}M$  remains the strongest. The positions of the soft mode minima are not significantly affected by  $U_{\text{eff}}$ . The 2H-polytype is not dynamically stable either with a minimum at  $(\frac{1}{3}, 0)$  ( $\frac{2}{3}M$ ), suggesting that it distorts into a  $3 \times 3$  or  $3 \times 1$  supercell. Adding a Hubbard- $U$  introduces additional instabilities at the M point, resulting in complex phonon spectra. However, since 2H-VSe<sub>2</sub> has not been synthesized yet and since it is predicted to have a fairly high magnetic transition temperature, it is unknown whether it would undergo this CDW transition from the non-magnetic state or if it would become ferromagnetic first, in which case would remain undistorted.

Angle-resolved photoelectron spectroscopy (ARPES) revealed that bulk 1T-VSe<sub>2</sub> shows partial Fermi surfaces nesting with a nesting vector of  $(\frac{1}{4}, \frac{1}{4})$ .<sup>94,95</sup> The Fermi surface of non-magnetic 1T-VSe<sub>2</sub> monolayers (shown in Figure 10) is of similar shape as the in-plane Fermi surface determined experimentally for bulk 1T-VSe<sub>2</sub>. Along with the similar phonon spectra, this suggests that the in-plane distortions of the CDW structure are not significantly affected by the dimensionality of VSe<sub>2</sub>. Partial nesting can be observed inside the cigar-like electron Fermi surface pockets. The nesting vectors (gray arrows in Figure 10) have the coordinates  $(\frac{1}{4}, \frac{1}{4})$ , which is consistent with the CDW supercell found in bulk and with the soft modes in our phonon spectra. The CDW transition in monolayer 1T-VSe<sub>2</sub> is thus consistent with a Fermi surface nesting mechanism.

To obtain a possible CDW structure, we followed the eigenvectors of the soft phonon mode. Using the MODULATION tag in PHONOPY, we created distorted structures along the  $\mathbf{q}$ -points  $(\frac{1}{4}, 0)$  and  $(\frac{1}{4}, \frac{1}{4})$ , and by using a superposition of the  $\mathbf{q}$ -points  $(\frac{1}{4}, 0)$  and  $(0, \frac{1}{4})$ . The structures were then relaxed using non-magnetic, ferromag-

netic, and antiferromagnetic spin configurations. The most stable structure was found using the superposition and is 82 meV/f.u. more stable than undistorted non-magnetic 1T-VSe<sub>2</sub>. It has a complex ferrimagnetic order with a total magnetization of approximately  $2 \mu_B/\text{cell}$  ( $0.12 \mu_B/\text{V atom}$ ). The magnetic moments of the individual V atoms all between  $1.05 \mu_B$  and  $1.25 \mu_B$  except for one atom that has a magnetic moment of  $0.86 \mu_B$ . Interestingly, initializing the calculations with both antiferromagnetic and ferromagnetic order led to ferrimagnetic spin order in the final structure.

Figure 11a shows the spin densities around the V atoms of the most stable structure. The minority spin atoms (light blue) form a chain of edge-sharing and corner-sharing triangles. Parallel to this chain, the minority spin densities form hexagons that are bridged by a single V atom. The V atom inside the hexagon has antiparallel spin and is the atom with the small magnetic moment of  $0.86 \mu_B$ . These structural features can also be observed in the inter-atomic distances (see Figure 11b). Inside the chains, most V-V distances are shorter than the  $a$ -axis lattice parameter  $a'$  of the undistorted non-magnetic 1T-VSe<sub>2</sub> monolayer ( $3.37 \text{ \AA}$ ). The shortest distances ( $3.19$  and  $3.24 \text{ \AA}$ ) can be found in triangular clusters inside the majority spin chains. The chains themselves are spatially separated by at least  $3.41 \text{ \AA}$ . Figure 11c shows how these features propagate throughout the crystal. The modulation wavelength in each direction is  $4a'$ , which is consistent with scanning tunneling microscopy (STM) measurements and the CDW vectors found in ARPES experiments.<sup>46,92-95</sup>

The in-plane distortions also lead to distorted VSe<sub>6</sub> units. In undistorted VSe<sub>2</sub>, the nearest neighbor V-Se distances are all approximately  $2.51 \text{ \AA}$ . In the distorted structure, only the V atom inside the hexagon has an undistorted coordination shell, and the spin density around it has the same shape as the V atoms in the antiferromagnetic structures (see Figure 3c). The coordination shells around the other atoms are strongly distorted, especially around the V atoms in the small triangles and the hexagon corners where V-Se distances as short as  $2.48$  and as long as  $2.56 \text{ \AA}$  can be found in the same coordination shell. These distortions change the crystal field around the V atoms, which lifts the degeneracy of bands. Figure 11d shows the band structures of non-magnetic and distorted 1T-VSe<sub>2</sub> monolayers. Non-magnetic 1T-VSe<sub>2</sub> is metallic with large electron pockets around the M point. The distorted structure on the other hand is a half-metal with small electron pockets near the  $\Gamma$  point in the minority spin channel. The majority spin channel shows no Fermi level crossings. This change in the band structure is consistent with electronic transport properties in ferecrystals and in bulk VSe<sub>2</sub> where a sharp increase in the Hall coefficient was observed and attributed to a reduction in carrier concentration without becoming insulating.<sup>40,48,49,52,56,83,96</sup> The periodic structural distortions along with the opening of band gaps indicate a Peierls-type transition at low temperatures.

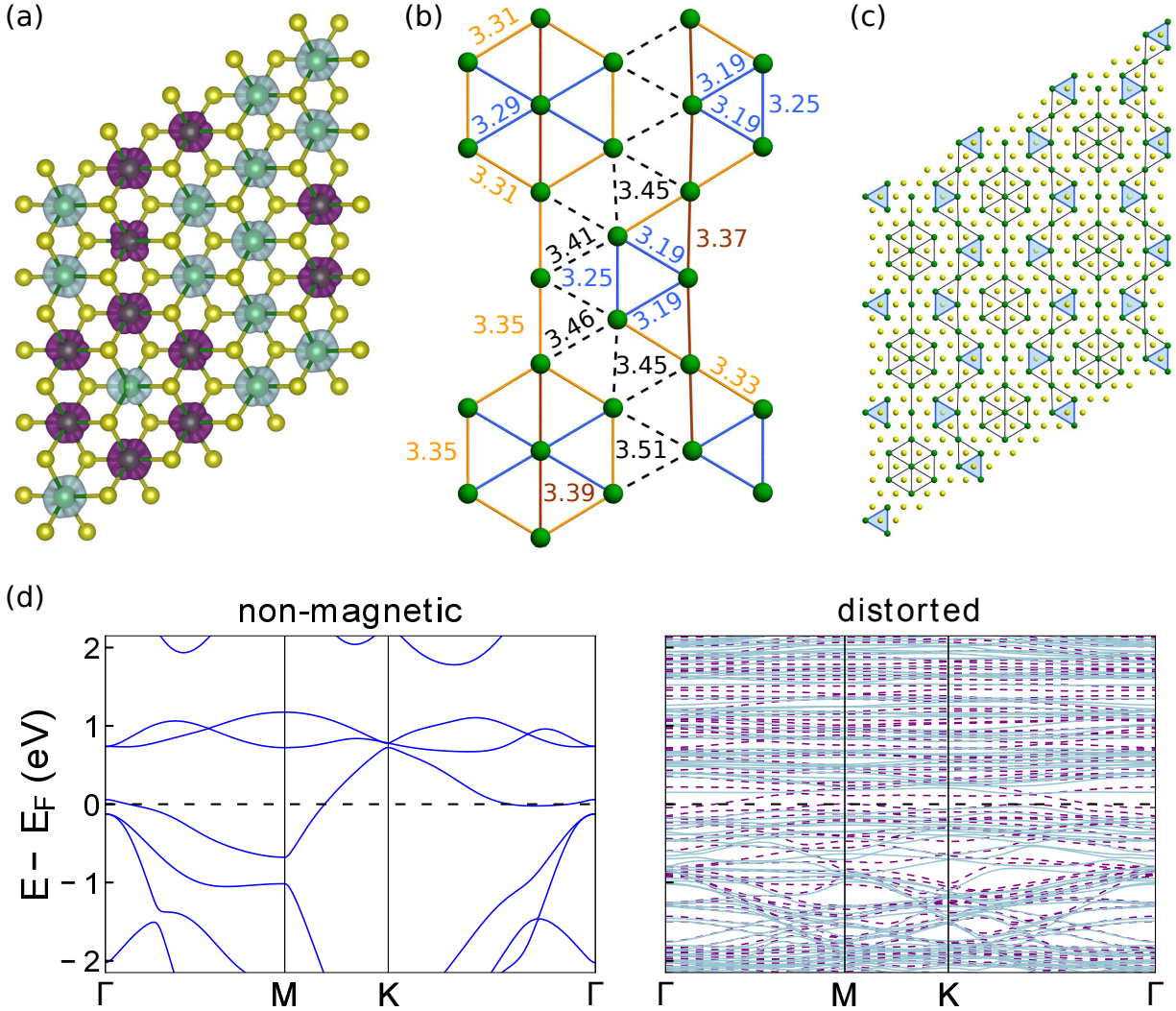


FIG. 11. (a) Unit cell of the most stable distorted structure of monolayer 1T-VSe<sub>2</sub>. The spin densities around the V atoms are shown in light blue and dark purple for the majority and minority spins, respectively. V atoms are dark green and Se atoms are light yellow. The isosurface values are set to  $0.01 e/a_0^3$  where  $a_0$  is the Bohr radius. (b) Detailed view of the chains of hexagons and triangles with V-V distances given in Ångström. Distances of less than 3.30, 3.35, and 3.40 Å are shown in blue, orange, and brown, respectively. Larger distances are shown in black dashed lines. Se atoms are omitted for clarity. (c) Top view onto a  $3 \times 3$  supercell of the distorted 1T-VSe<sub>2</sub> monolayer. Connected V atoms are less than 3.4 Å apart. Small area triangular V clusters are highlighted blue (see text). (d) Band structures of undistorted non-magnetic and distorted 1T-VSe<sub>2</sub> monolayers. For the distorted structure, solid light blue lines represent majority spin bands and dashed purple lines represent minority spin bands.

Comparing the magnetic properties with experimental data is challenging. Apart from that the monolayer may have different magnetic properties than the bulk, the magnetic properties of bulk 1T-VSe<sub>2</sub> in the CDW phase are not fully resolved because stoichiometric VSe<sub>2</sub> has not been synthesized yet. In the non-stoichiometric compounds, an increase in the magnetic susceptibility below the CDW transition temperature was observed, and it was discussed whether this increase is due to interstitial V atoms.<sup>41,48,49</sup> Ferrimagnetism or spin density waves (SDWs) were never considered. The calculated spin densities in Figure 11a suggest that in the mono-

layer, there is potential for a SDW. For a definitive answer, more experimental data on the magnetic properties in the CDW state is needed. Determining magnetic properties in misfit-layer compounds and ferecrystals containing VSe<sub>2</sub> monolayers and spin-polarized STM measurements on VSe<sub>2</sub> would give crucial information on the spin structure below the CDW transition temperature. Future computational research should focus on SDW structures for further insights into a potential SDW structure.

#### IV. CONCLUSION AND OUTLOOK

It was shown using density functional theory including the Hubbard- $U$  parameter that the ground state of two-dimensional VSe<sub>2</sub> is ferromagnetic for monolayers and that for bilayers, the ferromagnetic and an antiferromagnetic configuration are energetically nearly degenerate due to weak magnetic interactions between the layers. The VSe<sub>2</sub> monolayers exhibit an easy magnetization plane and belong to the family of  $XY$  magnets, but the transition temperature for 1T-VSe<sub>2</sub> is below the experimentally observed charge density wave (CDW) transition temperature. 1T-VSe<sub>2</sub> displays a charge density wave in bulk, in few layer nanosheets and in ferecrystals. The ferromagnetic monolayers are dynamically stable with the exception of 1T-VSe<sub>2</sub> for some  $U_{\text{eff}}$  values. The non-magnetic layers are unstable with a  $4\times 4$  supercell and a  $3\times 3$  supercell for the 1T and 2H-polytype, respectively. Within the  $ab$ -plane, non-magnetic 1T-VSe<sub>2</sub> monolayers show partial Fermi surface nesting similar to the bulk compound. The dynamic instability causes Peierls-type distortions in 1T-VSe<sub>2</sub> monolayers, which can also be observed in the electronic structure. The magnetic struc-

ture of this distorted phase is ferrimagnetic with a very small residual moment and indicates a potential spin density wave (SDW) structure. Future research should explore SDW structures in  $4\times 4$  1T-VSe<sub>2</sub> supercells. However, methods beyond DFT such as dynamical mean field theory may be necessary to fully describe the properties of VSe<sub>2</sub>.

#### ACKNOWLEDGMENTS

M.E. gratefully acknowledges Joshua Gabriel and Michael Ashton (University of Florida), and Arunima Singh (Lawrence Berkeley National Laboratory) for their assistance with magnetic anisotropy and phonon calculations, and Christian Schön (Max-Planck-Institut für Festkörperforschung in Stuttgart) for helpful discussions. The authors acknowledge the University of Oregon ACISS cluster (National Science Foundation OCI-0960354) and the University of Florida Research Computing system for computing resources. M.E. and D.C.J. acknowledge support from the National Science Foundation under grant DMR-1266217, and R.G.H. acknowledges support from the National Science Foundation under grant DMR-15242776.

- 
- <sup>1</sup> K. S. Novoselov, A. K. Geim, S. V. Morozov, D. Jiang, Y. Zhang, S. V. Dubonos, I. V. Grigorieva, and A. A. Firsov, *Science* **306**, 666 (2004).
- <sup>2</sup> K. S. Novoselov, D. Jiang, F. Schedin, T. J. Booth, V. V. Khotkevich, S. V. Morozov, and A. K. Geim, *Proc. Natl. Acad. Sci.* **102**, 10451 (2005).
- <sup>3</sup> A. Geim and K. Novoselov, *Nat. Mater.* **6**, 183 (2007).
- <sup>4</sup> X. Duan, C. Wang, A. Pan, R. Yu, and X. Duan, *Chem. Soc. Rev.* **44**, 8859 (2015).
- <sup>5</sup> M. Chhowalla, H. S. Shin, G. Eda, L.-J. Li, K. P. Loh, and H. Zhang, *Nat. Chem.* **5**, 263 (2013).
- <sup>6</sup> S. Lebègue and O. Eriksson, *Phys. Rev. B* **79**, 115409 (2009).
- <sup>7</sup> A. Kuc, N. Zibouche, and T. Heine, *Phys. Rev. B* **83**, 245213 (2011).
- <sup>8</sup> D. Xiao, G.-B. Liu, W. Feng, X. Xu, and W. Yao, *Phys. Rev. Lett.* **108**, 196802 (2012).
- <sup>9</sup> H. L. Zhuang and R. G. Hennig, *J. Phys. Chem. C* **117**, 20440 (2013).
- <sup>10</sup> C.-Y. Wang and G.-Y. Guo, *J. Phys. Chem. C* **119**, 13268 (2015).
- <sup>11</sup> H. Wang, H. Yuan, S. Sae Hong, Y. Li, and Y. Cui, *Chem. Soc. Rev.* **44**, 2664 (2015).
- <sup>12</sup> M. Pandey, A. Vojvodic, K. S. Thygesen, and K. W. Jacobsen, *J. Phys. Chem. Lett.* **6**, 1577 (2015).
- <sup>13</sup> D. Voiry, A. Mohite, and M. Chhowalla, *Chem. Soc. Rev.* **44**, 2702 (2015).
- <sup>14</sup> A. E. Maniadaki, G. Kopidakis, and I. N. Remediakis, *Solid State Commun.* **227**, 33 (2016).
- <sup>15</sup> W. Li and J. Li, *Nat. Commun.* **7**, 10843 (2016).
- <sup>16</sup> T. L. Tan, M. F. Ng, and G. Eda, *J. Phys. Chem. C* **120**, 2501 (2016).
- <sup>17</sup> J. Zhou and Q. Sun, *J. Am. Chem. Soc.* **133**, 15113 (2011).
- <sup>18</sup> Y. Zhou, Z. Wang, P. Yang, X. Zu, L. Yang, X. Sun, and F. Gao, *ACS Nano* **6**, 9727 (2012).
- <sup>19</sup> H. Zhang, L.-M. Liu, and W.-M. Lau, *J. Mater. Chem. A* **1**, 10821 (2013).
- <sup>20</sup> M. Kan, J. Zhou, Q. Sun, Y. Kawazoe, and P. Jena, *J. Phys. Chem. Lett.* **4**, 3382 (2013).
- <sup>21</sup> S. Zhang, Y. Li, T. Zhao, and Q. Wang, *Sci. Rep.* **4**, 5241 (2014).
- <sup>22</sup> M. Kan, S. Adhikari, and Q. Sun, *Phys. Chem. Chem. Phys.* **16**, 4990 (2014).
- <sup>23</sup> X. Li and J. Yang, *J. Mater. Chem. C* **2**, 7071 (2014).
- <sup>24</sup> Y. Ma, Y. Dai, M. Guo, C. Niu, Y. Zhu, and B. Huang, *ACS Nano* **6**, 1695 (2012).
- <sup>25</sup> H. Guo, N. Lu, L. Wang, X. Wu, and X. C. Zeng, *J. Phys. Chem. C* **118**, 7242 (2014).
- <sup>26</sup> H. Y. Lv, W. J. Lu, D. F. Shao, Y. Liu, and Y. P. Sun, *Phys. Rev. B* **92**, 214419 (2015).
- <sup>27</sup> P. Manchanda, V. Sharma, H. Yu, D. J. Sellmyer, and R. Skomski, *Appl. Phys. Lett.* **107**, 032402 (2015).
- <sup>28</sup> H. Pan, *J. Phys. Chem. C* **118**, 13248 (2014).
- <sup>29</sup> Y. Zhou, C. Yang, X. Xiang, and X. Zu, *Phys. Chem. Chem. Phys.* **15**, 14202 (2013).
- <sup>30</sup> F. Li, K. Tu, and Z. Chen, *J. Phys. Chem. C* **118**, 21264 (2014).
- <sup>31</sup> A. H. M. A. Wasey, S. Chakrabarty, and G. P. Das, *J. Appl. Phys.* **117**, 064313 (2015).
- <sup>32</sup> H. L. Zhuang and R. G. Hennig, *Phys. Rev. B* **93**, 054429 (2016).
- <sup>33</sup> X. O. Fex, G. Xiang, M. Lan, Y. Nie, D. Yang, and X. Zhang, *RSC Adv.* **6**, 31758 (2016).

- <sup>34</sup> S. Lebègue, T. Björkman, M. Klintonberg, R. M. Nieminen, and O. Eriksson, *Phys. Rev. X* **3**, 031002 (2013).
- <sup>35</sup> A. H. Thompson, J. C. Scanlon, and C. R. Symon, *Solid State Ionics* **1**, 47 (1980).
- <sup>36</sup> H. I. Starnberg, H. E. Brauer, L. J. Holleboom, and H. P. Hughes, *Phys. Rev. Lett.* **70**, 3111 (1993).
- <sup>37</sup> H. E. Brauer, H. I. Starnberg, L. J. Holleboom, and H. P. Hughes, *Surf. Sci.* **331** – **333**, 419 (1995).
- <sup>38</sup> H. E. Brauer, I. Ekvall, H. Olin, H. I. Starnberg, E. Wahlström, H. P. Hughes, and V. N. Strocov, *Phys. Rev. B* **55**, 10022 (1997).
- <sup>39</sup> I. Ekvall, H. E. Brauer, H. Olin, H. I. Starnberg, and E. Wahlström, *Appl. Phys. A* **66**, S197 (1998).
- <sup>40</sup> A. H. Thompson and B. G. Silbernagel, *Phys. Rev. B* **19**, 3420 (1979).
- <sup>41</sup> L. F. Schneemeyer, A. Stacy, and M. J. Sienko, *Inorg. Chem.* **19**, 2659 (1980).
- <sup>42</sup> B. Giambattista, C. G. Slough, W. W. McNairy, and R. V. Coleman, *Phys. Rev. B* **41**, 10082 (1990).
- <sup>43</sup> G. V. Kamarchuk, A. V. Khotkevich, V. M. Bagatsky, V. G. Ivanov, P. Molinié, A. Leblanc, and E. Faulques, *Phys. Rev. B* **63**, 073107 (2001).
- <sup>44</sup> I. A. Gospodarev, A. V. Eremenko, T. V. Ignatova, G. V. Kamarchuk, I. G. Kolobov, P. A. Minaev, E. S. Syrkin, S. B. Feodosyev, V. D. Fil, A. Soreau-Leblanc, P. Molinie, and E. C. Faulques, *Low Temp. Phys.* **29**, 151 (2003).
- <sup>45</sup> K. Horiba, K. Ono, J. H. Oh, T. Kihara, S. Nakazono, M. Oshima, O. Shiino, H. W. Yeom, A. Kakizaki, and Y. Aiura, *Phys. Rev. B* **68**, 155108 (2003).
- <sup>46</sup> D. J. Eaglesham, R. L. Withers, and D. M. Bird, *J. Phys. C: Solid State Phys.* **19**, 359 (1986).
- <sup>47</sup> K. Xu, P. Chen, X. Li, C. Wu, Y. Guo, J. Zhao, X. Wu, and Y. Xie, *Angew. Chemie Int. Ed.* **52**, 10477 (2013).
- <sup>48</sup> M. Bayard and M. J. Sienko, *J. Solid State Chem.* **19**, 325 (1976).
- <sup>49</sup> C. F. van Bruggen and C. Haas, *Solid State Commun.* **20**, 251 (1976).
- <sup>50</sup> A. H. Thompson and B. G. Silbernagel, *J. Appl. Phys.* **49**, 1477 (1978).
- <sup>51</sup> G. A. Wieggers, *Prog. Solid State Chem.* **24**, 1 (1996).
- <sup>52</sup> R. Atkins, S. Disch, Z. Jones, I. Häusler, C. Grosse, S. F. Fischer, W. Neumann, P. Zschack, and D. C. Johnson, *J. Solid State Chem.* **202**, 128 (2013).
- <sup>53</sup> R. Atkins, M. Dolgos, A. Fiedler, C. Grosse, S. F. Fischer, S. P. Rudin, and D. C. Johnson, *Chem. Mater.* **26**, 2862 (2014).
- <sup>54</sup> M. B. Alemayehu, M. Falmbigl, K. Ta, J. Ditto, D. L. Medlin, and D. C. Johnson, *Angew. Chemie Int. Ed.* **54**, 15468 (2015).
- <sup>55</sup> M. Falmbigl, D. Putzky, J. Ditto, M. Esters, S. R. Bauers, F. Ronning, and D. C. Johnson, *ACS Nano* **9**, 8440 (2015).
- <sup>56</sup> M. Falmbigl, A. Fiedler, R. E. Atkins, S. F. Fischer, and D. C. Johnson, *Nano Lett.* **15**, 943 (2015).
- <sup>57</sup> P.-R. Huang, Y. He, H. K. Pal, and M. Kindermann, (2015).
- <sup>58</sup> G. Kresse and J. Hafner, *Phys. Rev. B* **49**, 14251 (1994).
- <sup>59</sup> G. Kresse and J. Furthmüller, *Comput. Mat. Sci.* **6**, 15 (1996).
- <sup>60</sup> G. Kresse and J. Furthmüller, *Phys. Rev. B* **54**, 11169 (1996).
- <sup>61</sup> P. E. Blöchl, *Phys. Rev. B* **50**, 17953 (1994).
- <sup>62</sup> G. Kresse and D. Joubert, *Phys. Rev. B* **59**, 1758 (1999).
- <sup>63</sup> J. P. Perdew and A. Zunger, *Phys. Rev. B* **23**, 5048 (1981).
- <sup>64</sup> J. P. Perdew, K. Burke, and M. Ernzerhof, *Phys. Rev. Lett.* **77**, 3865 (1996).
- <sup>65</sup> J. Heyd, G. E. Scuseria, and M. Ernzerhof, *J. Chem. Phys.* **118**, 8207 (2003).
- <sup>66</sup> S. L. Dudarev, G. A. Botton, S. Y. Savrasov, C. J. Humphreys, and A. P. Sutton, *Phys. Rev. B* **57**, 1505 (1998).
- <sup>67</sup> A. Tkatchenko and M. Scheffler, *Phys. Rev. Lett.* **102**, 073005 (2009).
- <sup>68</sup> A. Tkatchenko, R. A. DiStasio, R. Car, and M. Scheffler, *Phys. Rev. Lett.* **108**, 236402 (2012).
- <sup>69</sup> S. Grimme, *J. Comput. Chem.* **27**, 1787 (2006).
- <sup>70</sup> T. Bučko, J. Hafner, S. Lebègue, and J. G. Ángyán, *J. Phys. Chem. A* **114**, 11814 (2010).
- <sup>71</sup> M. Dion, H. Rydberg, E. Schröder, D. C. Langreth, and B. I. Lundqvist, *Phys. Rev. Lett.* **92**, 246401 (2004).
- <sup>72</sup> G. Román-Pérez and J. M. Soler, *Phys. Rev. Lett.* **103**, 096102 (2009).
- <sup>73</sup> J. Klimeš, D. R. Bowler, and A. Michaelides, *J. Phys. Condens. Matter* **22**, 022201 (2010).
- <sup>74</sup> J. Klimeš, D. R. Bowler, and A. Michaelides, *Phys. Rev. B* **83**, 195131 (2011).
- <sup>75</sup> H. J. Monkhorst and J. D. Pack, *Phys. Rev. B* **13**, 5188 (1976).
- <sup>76</sup> S. P. Ong, W. D. Richards, A. Jain, G. Hautier, M. Kocher, S. Cholia, D. Gunter, V. L. Chevrier, K. A. Persson, and G. Ceder, *Comput. Mater. Sci.* **68**, 314 (2013).
- <sup>77</sup> K. Mathew, A. K. Singh, J. J. Gabriel, K. Choudhary, S. B. Sinnott, A. V. Davydov, F. Tavazza, and R. G. Hennig, *Comput. Mater. Sci.* **122**, 183 (2016).
- <sup>78</sup> K. Momma and F. Izumi, *J. Appl. Crystallogr.* **44**, 1272 (2011).
- <sup>79</sup> A. A. Mostofi, J. R. Yates, G. Pizzi, Y.-S. Lee, I. Souza, D. Vanderbilt, and N. Marzari, *Comp. Phys. Commun.* **185**, 2309 (2014).
- <sup>80</sup> A. Kokalj, *Comp. Mater. Sci.* **28**, 155 (2003).
- <sup>81</sup> See Supplemental Material at [URL will be added by the publisher] for the  $U_{\text{eff}}$  dependence of the total energies, magnetizations, and  $a$ -axis lattice parameters for 1T- and 2H-VSe<sub>2</sub> in monolayers, bilayers and bulk, for the optB86b band structure, and results of select bulk calculations, which includes Ref. [97].
- <sup>82</sup> E. B. Isaacs and C. A. Marianetti, *Phys. Rev. B* **94**, 035120 (2016).
- <sup>83</sup> O. K. Hite, M. Falmbigl, M. B. Alemayehu, M. Esters, S. R. Wood, and D. C. Johnson, *Chem. Mater.* **29**, 5646 (2017).
- <sup>84</sup> H. Schmidt, F. Giustiniano, and G. Eda, *Chem. Soc. Rev.* **44**, 7715 (2015).
- <sup>85</sup> Y. Zhang, T.-R. Chang, B. Zhou, Y.-T. Cui, H. Yan, Z. Liu, F. Schmitt, J. Lee, R. Moore, Y. Chen, H. Lin, H.-T. Jeng, S.-K. Mo, Z. Hussain, A. Bansil, and Z.-X. Shen, *Nat. Nanotechnol.* **9**, 111 (2014).
- <sup>86</sup> A. Splendiani, L. Sun, Y. Zhang, T. Li, J. Kim, C. Y. Chim, G. Galli, and F. Wang, *Nano Lett.* **10**, 1271 (2010).
- <sup>87</sup> M. H. Whangbo and E. Canadell, *J. Am. Chem. Soc.* **114**, 9587 (1992).
- <sup>88</sup> M. Calandra, I. I. Mazin, and F. Mauri, *Phys. Rev. B* **80**, 241108(R) (2009).
- <sup>89</sup> M. Falmbigl, Z. Hay, J. Ditto, G. Mitchson, and D. C. Johnson, *J. Mater. Chem. C* **3**, 12308 (2015).
- <sup>90</sup> J. F. Fernández, M. F. Ferreira, and J. Stankiewicz, *Phys. Rev. B* **34**, 292 (1986).

- <sup>91</sup> A. Togo and I. Tanaka, *Scr. Mater.* **108**, 1 (2015).
- <sup>92</sup> H. P. Hughes, C. Webb, and P. M. Williams, *J. Phys. C: Solid State Phys.* **13**, 1125 (1980).
- <sup>93</sup> J.-J. Kim, C. Park, and H. Olin, *J. Korean Phys. Soc.* **31**, 713 (1997).
- <sup>94</sup> K. Terashima, T. Sato, H. Komatsu, T. Takahashi, N. Maeda, and K. Hayashi, *Phys. Rev. B* **68**, 155108 (2003).
- <sup>95</sup> V. N. Strocov, M. Shi, M. Kobayashi, C. Monney, X. Wang, J. Krempasky, T. Schmitt, L. Patthey, H. Berger, and P. Blaha, *Phys. Rev. Lett.* **109**, 086401 (2012).
- <sup>96</sup> C. S. Yadav and A. K. Rastogi, *Solid State Commun.* **150**, 648 (2010).
- <sup>97</sup> D. Zhang, J. Ha, H. Baek, Y.-H. Chan, F. D. Natterer, A. F. Myers, J. D. Schumacher, W. G. Cullen, A. V. Davydov, Y. Kuk, M. Y. Chou, N. B. Zhitenev, and J. A. Stroscio, *Phys. Rev. Materials* **1**, 024005 (2017).